Final Technical Report

Submitted to the U.S. Geological Survey

Principal Investigators: John H. Shaw (Harvard) and James F. Dolan (USC)

Authors: Franklin Wolfe, John H. Shaw, and Andreas Plesch
Department of Earth & Planetary Sciences, Harvard University
Cambridge, MA 02138
Fax (617) 495-8839
wolfe_franklin@g.harvard.edu // 919 616-6756
shaw@eps.harvard.edu // 617 495-8008
andreas_plesch@harvard.edu // 617 495-2356
Daniel J. Ponti, Earthquake Hazards Program, United States Geological
Survey, Menlo Park, CA 94025
dponti@usgs.gov // 650 329-5679
James F. Dolan, Department of Earth Sciences, University of Southern
California, Los Angeles, CA 90089
dolan@usc.edu // 213 740-8599
Mark R. Legg, Legg Geophysical, Huntington Beach, CA 92647
mark@legggeo.com // 714 842-0404

Abstract
We developed a new 3D structural model of the Wilmington blind-thrust to serve as a basis for improved estimates of earthquake hazard in Southern California. 3D analysis of offshore seismic reflection profiles, petroleum and water wells, and recent mapping of groundwater aquifers in the southwestern Los Angeles basin indicate that the Wilmington blind-thrust fault is tectonically active and capable of generating large, damaging earthquakes. This overturns the long-held view that the fault became dormant in the Late Pliocene, barring its inclusion in state-of-the-art regional earthquake hazard assessments. The size of the fault suggests that it is capable of generating moderate-magnitude earthquakes (M 6.2-6.3), while potential linkages with other nearby faults (e.g., Huntington Beach, Torrance, Compton) pose the threat of larger, multi-segment events (M > 7). These earthquakes would directly impact the Ports of Los Angeles and Long Beach, as well as the broader Los Angeles metropolitan area.

Introduction
Several recent, highly destructive earthquakes on thrust and reverse faults (e.g., 1994 Northridge [M 6.7], California; 1999 Chi-Chi [M 7.6], Taiwan; 2001 Bhuj [7.6], India; 2009 Wenchuan [M 7.9], China; and 2015 Gorkha [M 7.7], Nepal; 2016 Kaikoura [M 7.8], New Zealand events) highlight the need to better address the seismic hazards posed by this class of structure to an increasingly urbanized global population. Characterizing the earthquake hazards of blind-thrust faults, in particular, poses a significant challenge, as these faults do not extend to the surface. Rather, near-surface deformation above these structures is accommodated primarily by folding, not faulting (Dolan et al., 2003; Pratt et al., 2002; Shaw et al., 2002; Shaw and Suppe, 1996, 1994; Stein and Ekström, 1992; Stein and King, 1984). The concealed nature of these faults, combined with a lack of established standards for defining their paleo-earthquake activity, has led to them being poorly represented in most regional seismic hazards assessments.

The Wilmington blind-thrust offers an extreme example of the ambiguity in hazard assessments of blind-thrust faults. The Wilmington fault is a large, northeast-dipping, blind-thrust ramp that underlies the southwestern Los Angeles basin in California (Figure 1). We consider this fault as part of the THUMS-Huntington Beach oblique-slip system (Ishutov, 2013; Legg and Prior, 2007; Wright, 1991). Displacement on this fault formed the overlying Wilmington anticline, which provides a structural trap for one of the largest petroleum fields in southern California. Although the larger THUMS-Huntington Beach system has been known for decades, the Wilmington blind-thrust is not currently included in state-of-the-art earthquake hazard assessments (e.g., UCERF3) (Field et al., 2013). This reflects a long-held view that the fault became tectonically inactive in the late Pliocene. Moreover, disagreement persists over many first-order characteristics of the fault, such as its sense of slip (Ishutov, 2013; Baher et al., 2005; Fisher et al., 2004; Davis and Namson, 1998; Wright, 1987; Truex, 1974).
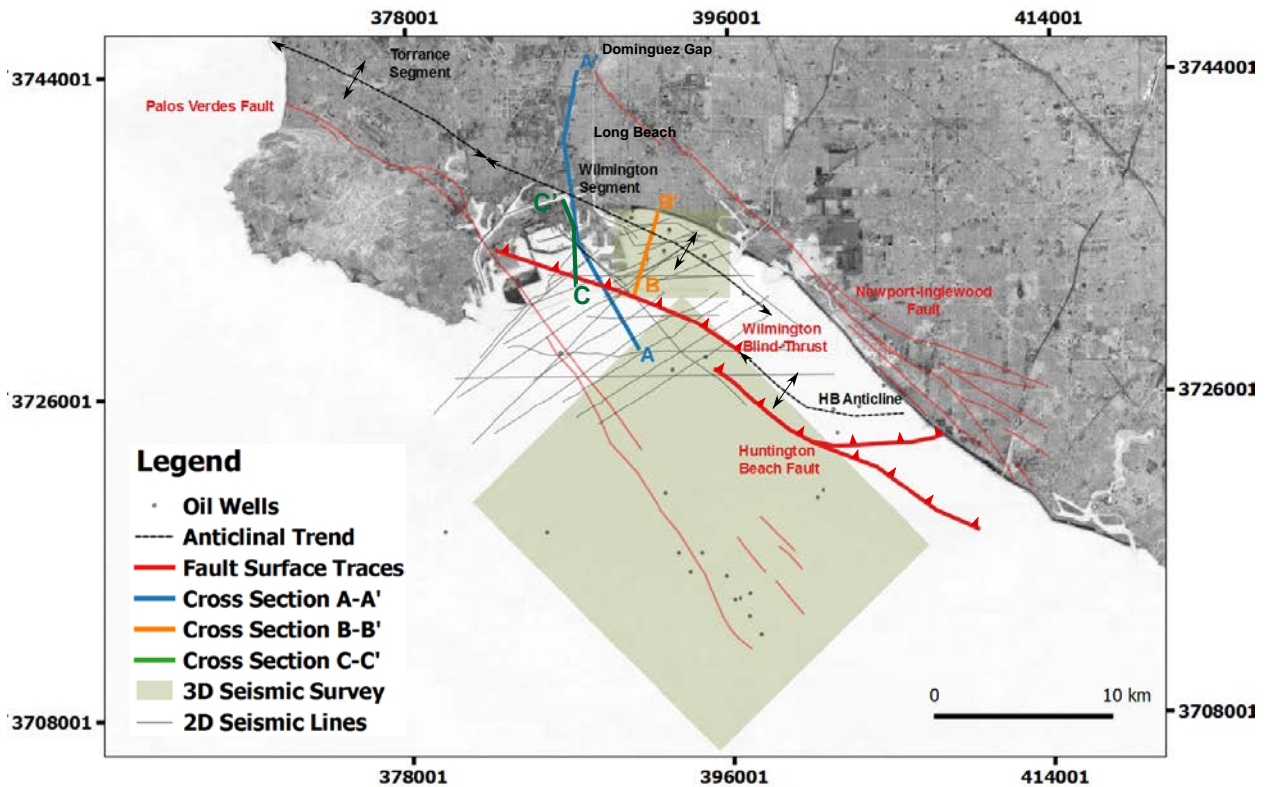
Figure 1. Location map for the study site. The two green boxes represent the areas of 3D seismic surveys used in this study. The grey lines denote select DOE Terralog, USGS (E-1-01-SC), and USGS (A-1-00-SC) 2D seismic surveys. Base image from Bing Maps.

Analysis of marine 2D and 3D seismic reflection data reveals that the Wilmington blind-thrust dips to the northeast beneath the oil field, where it offsets the top of the Catalina Schist basement by more than 1,200 meters (Figure 2). The fault slip decreases upward towards the tip of the fault, where it terminates into the lower Pliocene Repetto Formation (Figure 2). This is consistent with the fault tip imaged and interpreted by Ishutov (2013) and with displacement patterns of shear fault-propagation folds developed above blind-thrust faults (Hughes and Shaw, 2014; Allmendinger, 1998; Erslev, 1991; Suppe and Medwedeff, 1990). Based on a pronounced thinning of syn-tectonic sedimentary strata onto the crest of the fold, the structure formed in the Pliocene (Figure 2). Overlying upper Pliocene to lower Pleistocene horizons generally maintain their thickness above the fold crest, implying that the structure was inactive during this time. These observations have led to the long-held view that the Wilmington thrust is no longer tectonically active.
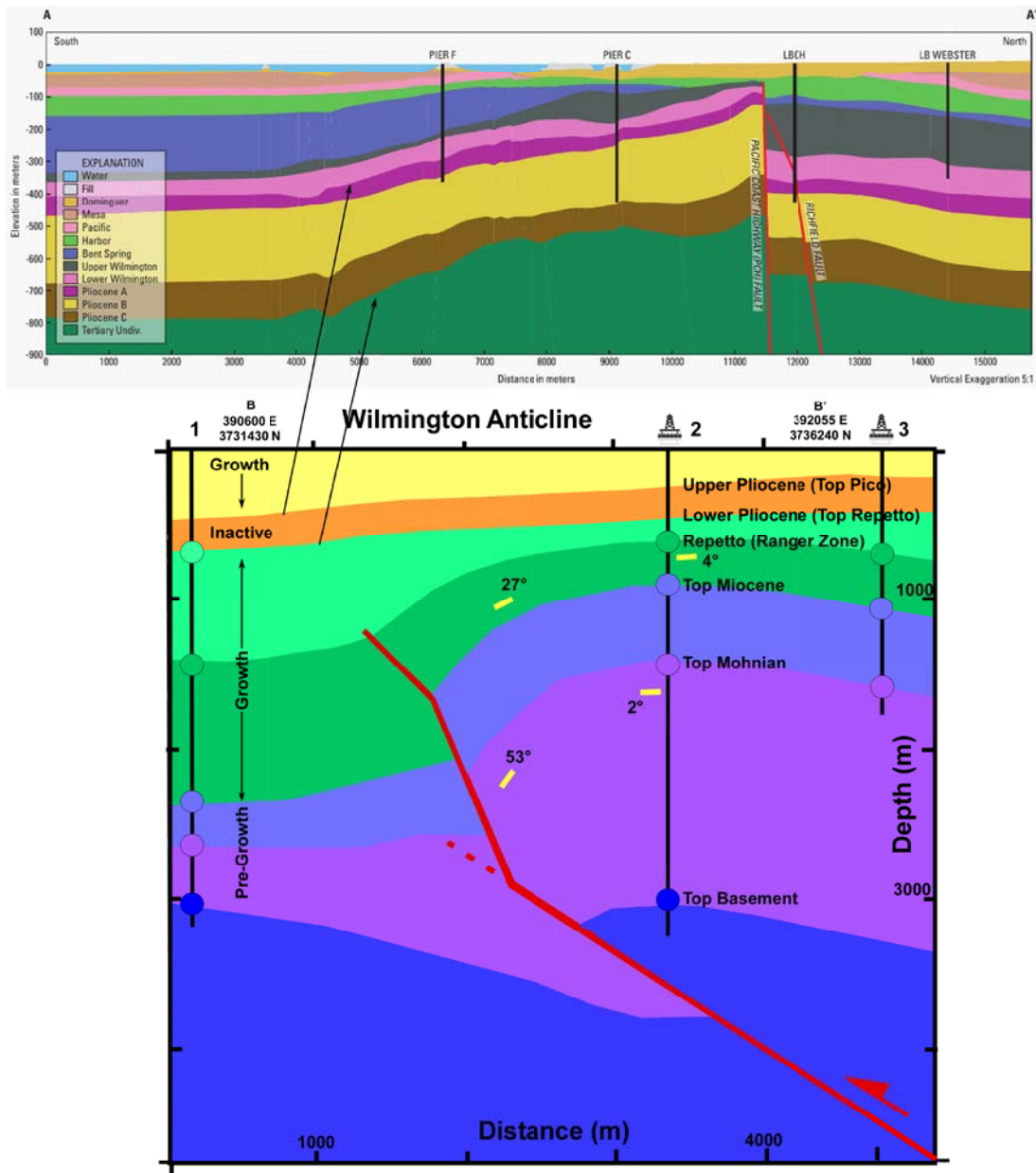
3

Figure 2. Linking shallow deformation to Wilmington blind-thrust. Onshore well transect from Ponti et al. (2007) (top) and geologic cross section built from interpretations of 3D seismic survey (bottom). Folded upper Pliocene and Quaternary strata in the cross section and uplift and thinning of upper Quaternary strata in the well profile suggest reactivation of the Wilmington blind-thrust. The geometry of the Wilmington blind-thrust is constrained by the 3D seismic data and other regional 2D sections. The Pliocene A and Tertiary Undiv. from A-A' correspond to Top of Pliocene horizon and Base Quaternary in B-B'. Dip meter data (yellow dip indicators) from various THUMS oil island deviated oil wells that penetrate this seismic section. Not all boreholes are shown for clarity. Locations for these two cross sections are shown in Figure 1. Location 1 corresponds to horizon ties

from BETA oil field wells. Well 2 (D-703) and 3 (C-813) correspond to horizon picks from THUMS oil islands published on the DOGGR website.

Evidence for Reactivation of the Wilmington Blind-Thrust
Two distinct lines of evidence suggest that the Wilmington structure was reactivated in the late Pleistocene. First, offshore 3D seismic reflection data image folding of upper Pliocene strata along a synclinal axial surface that is pinned at depth to the tipline of the Wilmington thrust (Figure 2). These folds exhibit more than 320 meters of relief, which implies about 600 meters of dip-slip on the underlying Wilmington thrust. Notably, these data do not image any thinning of shallow sedimentary units, implying that reactivation was very recent (i.e., reactivation occurred after the deposition of these units).

The second line of evidence for tectonic reactivation is found in the geometry of upper Quaternary strata in the onshore, southwestern Los Angeles basin. Ponti et al. (2007) developed a comprehensive sequence stratigraphic model for these Quaternary units in the Dominguez Gap region of Long Beach, which provides an exceptional framework to assess activity of the Wilmington thrust. A prominent feature in this stratigraphic model is broad anticlinal folding along a northwest trend that is associated with the Wilmington anticline. As illustrated by the well-based section across the structure (Figure 2), all but the youngest sedimentary units are structurally higher above the fold crest and increase in depth both to the northeast and southwest along the limbs of the Wilmington structure.

As noted by Ponti et al. (2007), the long hiatus associated with the boundary between the Pliocene A and Lower Wilmington sequences, without clear evidence of an angular unconformity between the two sequences, suggests that fold growth stopped in latest Pliocene to early Pleistocene time, between approximately 1.77 and 0.71 million years ago. This is consistent with the observation of no thickness changes within the upper Pliocene to lower Pleistocene strata across the fold crest imaged in the offshore geophysical profiles. Reactivation of the structure post ca. 571 ka is manifest in the thinning of upper Pleistocene units to the north onto the crest of the fold. A stratigraphic model of the Wilmington – Long Beach area by Ehman and Edwards (2017) also documents the prominent deformational patterns observed within these sequences (Ehman and Edwards, 2017).

To assess if the onshore and offshore constraints on recent folding are both reflective of activity on the Wilmington blind-thrust, we analyzed additional water and oil well data (i.e., formation top and dip meter), published cross sections, and seismic reflection surveys (2D and 3D). These data were geo-referenced and integrated into GOCAD, a computer-aided design tool used to build 3D surfaces of key horizons in the region (Mallet, 1992) (Figure 3). We then built a triangulated surface representation of the fault using the approach of Plesch et al. (2007) (Figure 3).
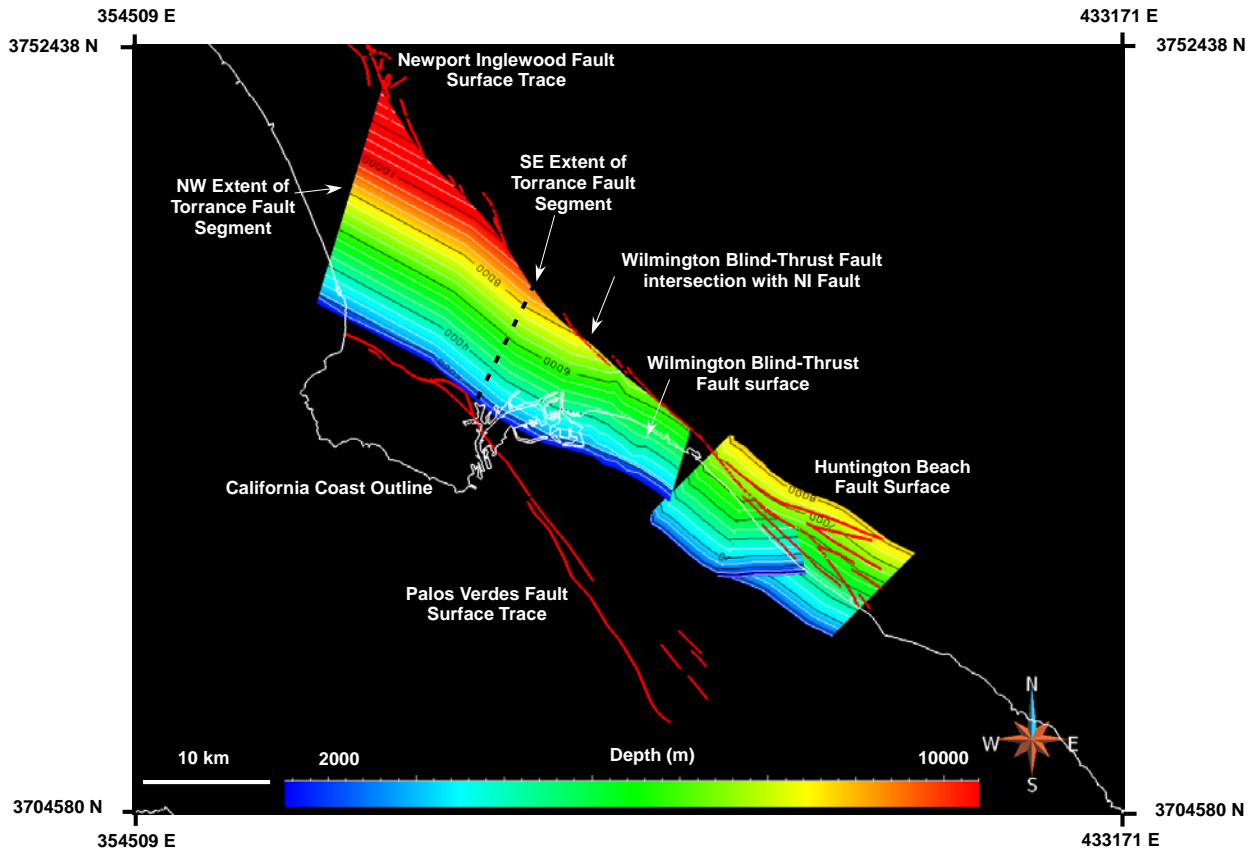
Figure. 3. Map view of the depth contoured fault surfaces (Wilmington Preferred Dip Model) described and used to calculate seismic hazard. The surface traces of the Palos Verdes and Newport Inglewood faults are also shown. The northeastern extent of the faults shown in this figure is the Newport Inglewood Fault surface (not pictured). Coordinates: NAD27/UTM Zone 11N.

A key finding from the new model is a direct linkage between the subsurface folding in the forelimb of the Wilmington anticline and the deformation of the shallow Pleistocene aquifers identified by Ponti et al. (2007) (Figure 4). As illustrated in Figure 3, the southwest limb of the Wilmington anticline, imaged in the 3D seismic reflection data and displayed in our 3D model, extends upward and directly corresponds with the fold limb identified by Ponti et al. (2007). Notably, the shallowest horizon, which is constrained by the 3D seismic reflection and petroleum well data (the Pliocene-C unit), is also mapped by Ponti et al. (2007) at the base of the deformed Pleistocene section. This offers a direct linkage between subsurface deformation in the Wilmington anticline and folding of upper Pleistocene sequences.
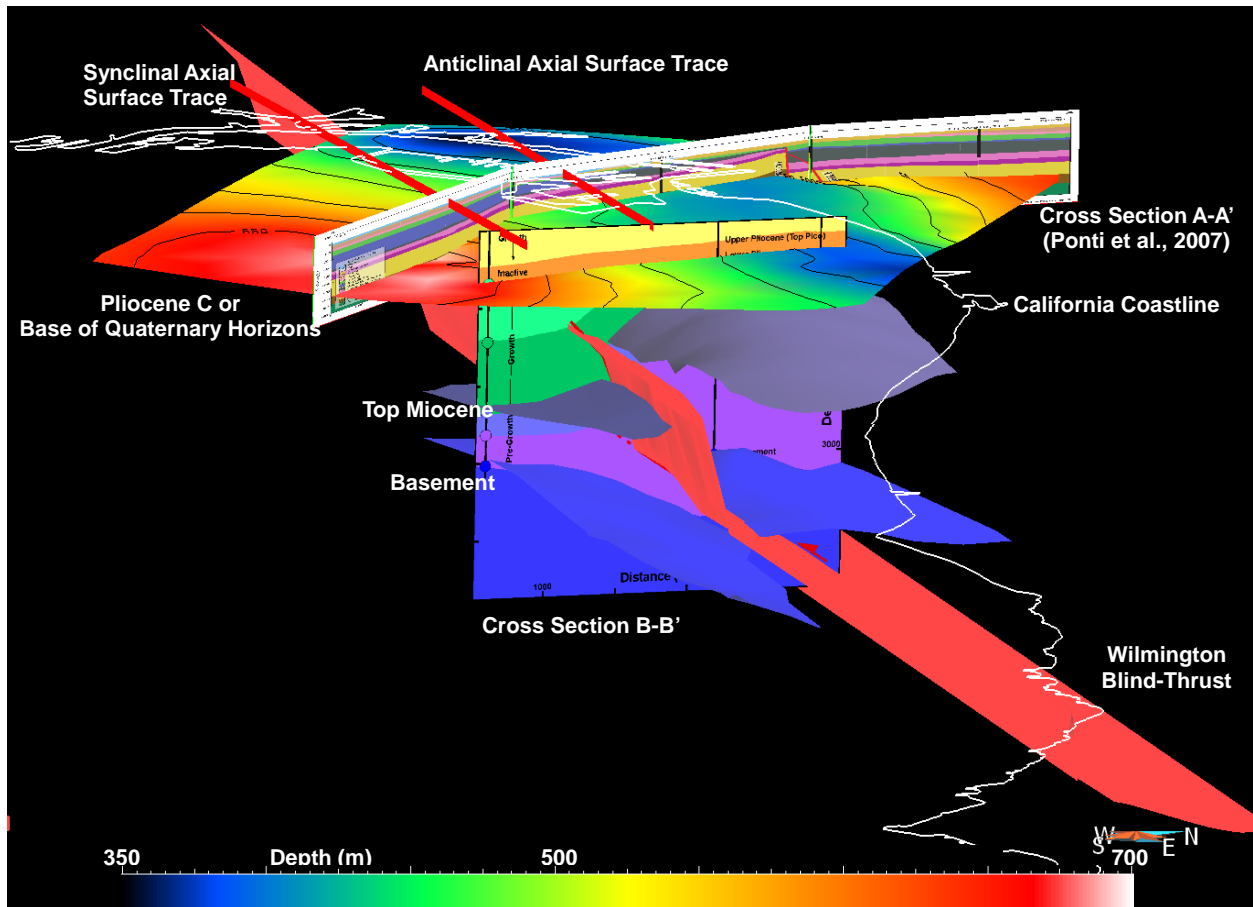
6

Figure 4. 3D Model of the Wilmington blind-thrust. 3D perspective of Wilmington anticline showing correspondence between Pliocene and Miocene horizons mapped from the offshore 3D seismic survey and folding of Pleistocene aquifers in cross section from Ponti et al. (2007) (Fig. 2). The depth color-contoured horizon is the Pliocene–C unit (base of Quaternary) that was mapped from the 2D seismic survey lines and corresponds to the dark brown unit in the Ponti et al. (2007) section (see Fig. 1). Red lines represent surface projections of synclinal and anticlinal axial surfaces correlated between the 3D seismic volume, 2D seismic lines, and published oil field data and cross sections.

The clearest examples of discrete forelimb deformation are within the Pacific (~40-117 ka) and Harbor sequences (~130-175 ka) (Figure 5). The youngest deformed sequence recognizable within this fold limb is the Mesa unit, which has an age of ~20-41 ka (McDougall et al., 2012; Ponti et al., 2007) (Figure 5). This clearly establishes late Pleistocene tectonic activity on the underlying Wilmington blind-thrust and motivated our efforts to further characterize this potential earthquake source.
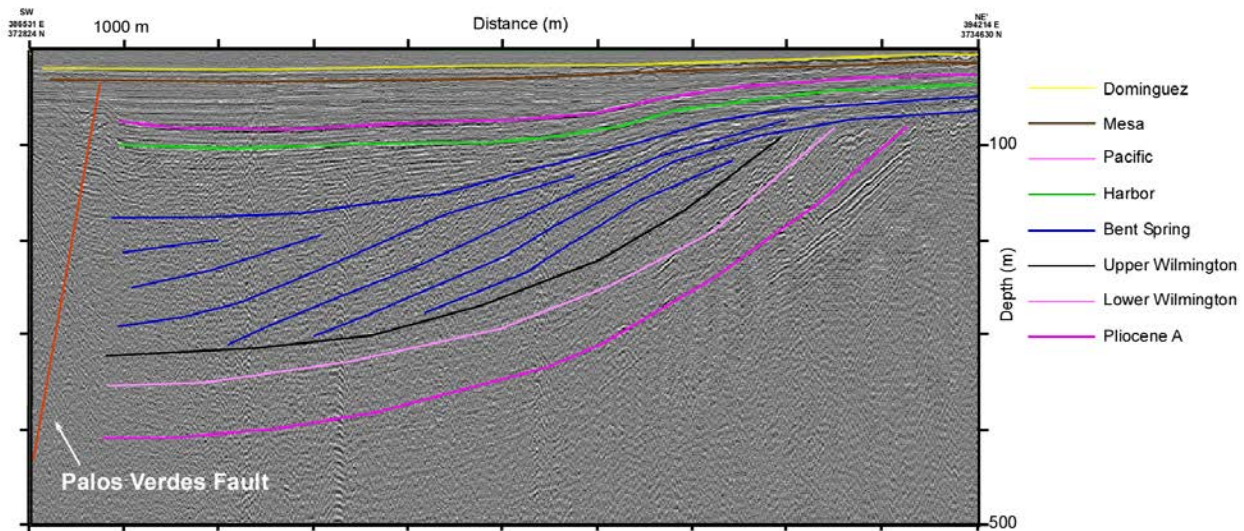
Figure 5. 10X Vertical Exaggeration. Folding and thinning of Quaternary strata imaged in 2D seismic survey lines across the strike of the Wilmington anticline. Clear forelimb folded panel interpreted in the Pacific (~40-117 ka) and Harbor (~130-175 ka) horizons, indicating that they were deformed by the underlying Wilmington blind-thrust. Clear thinning onto the crest of the Wilmington anticline is interpreted in the Bent Spring (~200-500 ka), Harbor, Pacific, Mesa (~20-41 ka), and Dominguez (<18 ka) formations, indicating that they were deposited syn-tectonically and that deformation has persisted in recent times. This is line 812 from the USGS A-1-00-SC seismic survey and is located along the same trend as B-B'.

Timing of Reactivation and Slip Rate

Our analysis of slip rates for Pliocene to Quaternary strata indicate a substantial increase in slip rate on the Wilmington blind-thrust post 1.77 Ma, following deposition of the Pliocene A horizon post (Figure 6). Slip rates were calculated by measuring the total structural relief onto the crest of the Wilmington anticline and correcting for regional basinward dip. Futher, 3D mapping of Quaternary strata reveal that units older than ~571 ka maintain thickness across the crest of the Wilmington anticline, indicating deposition during a period of tectonic quiescence. However, units younger than ~571 ka, including the overlying Bent Spring formation (~200-500 ka), thin onto the crest of the structure along the trend of the Wilmington anticline.

Together, these analyses suggest that the structure was reactivated following deposition of the Lower Wilmington formation (~620-710 ka), which is well-dated by the Lava Creek B ash deposited at ~639 ka (McDougall et al., 2012). This timing appears consistent with accelerated uplift of the Palos Verdes Anticlinorium (Francis and Legg, 2007). The pronounced thinning is demonstrated in all of the resolvable units younger than the Lower Wilmington, which suggests that the structure has remained active in recent times. This is in agreement with our calculated slip rates, which show increasing activity on the Wilmington blind-thrust to the present (Figure 6).
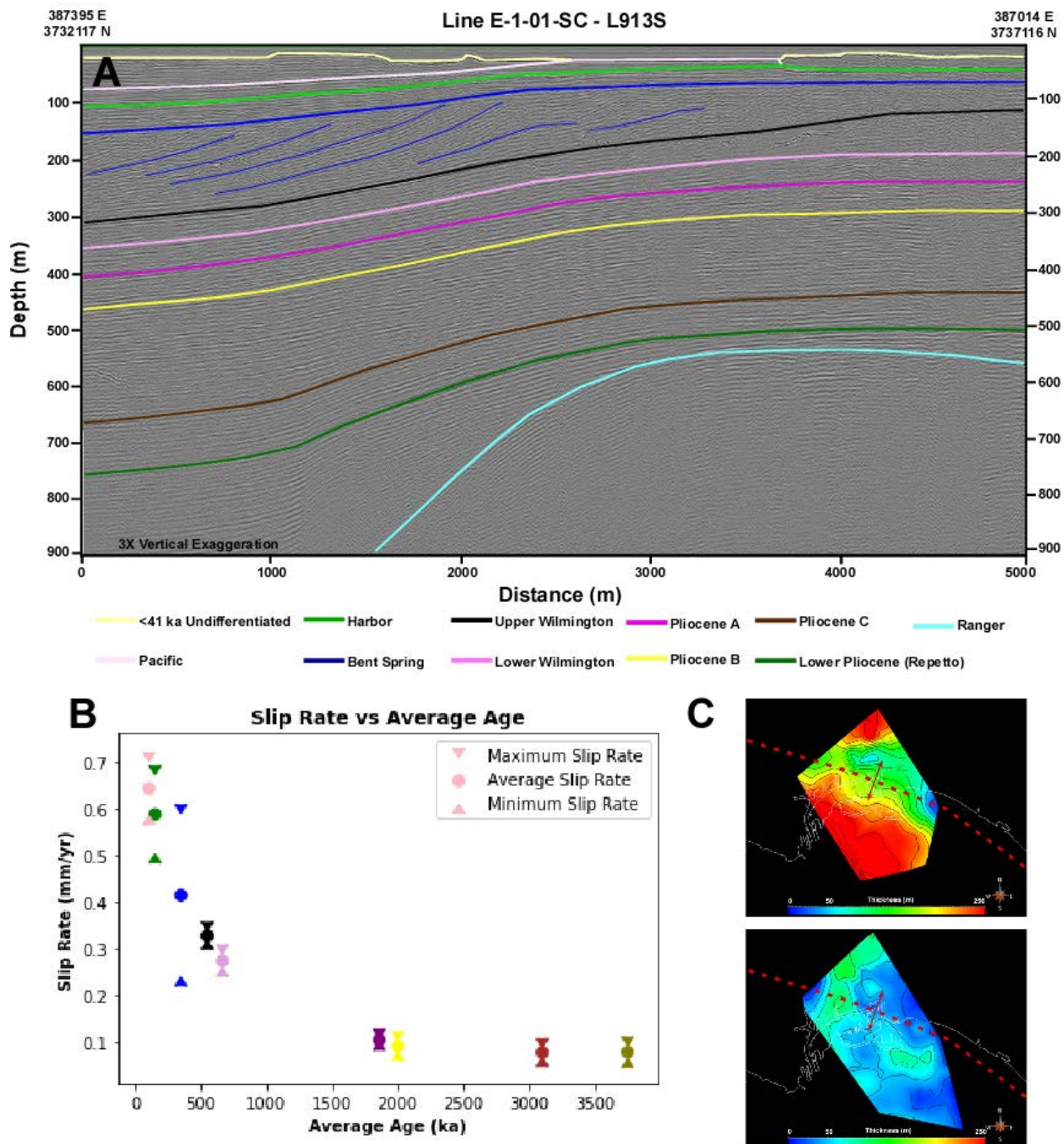
8

Figure 6. Timing of Reactivation. (A) Folding and thinning of Quaternary strata imaged in 2D seismic survey lines across the strike of the Wilmington anticline. Clear forelimb folded panel interpreted in the Pacific (~40-117 ka) and Harbor (~130-175 ka) horizons, indicating that they were deformed by the underlying Wilmington blind-thrust. Thinning onto the crest of the Wilmington anticline is interpreted in the Bent Spring (~200-500 ka), Harbor, Pacific, and <41 ka Undifferentiated formations, indicating that they were deposited syn-tectonically and that deformation has persisted in recent times. This is line L913S from the USGS E-1-01-SC seismic survey and is located along the same trend as C-C'. 3X Vertical Exaggeration. See Figure 1 for location. (B) Slip rates calculated by measuring the total structural relief of deformed strata and using the preferred fault dip of 32°. The horizon colors for the seismic

interpretation are the same for the slip rate data points. A clear inflection in slip rates occurs between deposition of the Pliocene A and Lower Wilmington formations, indicating that the Wilmington blind-thrust became active during this time. (C) Thickness map of the Bent Spring (~200-500 ka) and Lower Wilmington (~620-710 ka) formations. The Bent Spring formation shown in the upper image thins onto the crest of the structure and thickens into the forelimb and backlimbs, indicating it was deposited syn-tectonically, whereas the Lower Wilmington formation shown in the lower image does not show this trend, indicating it was deposited during the period of tectonic quiescence. Red lines and arrows are position of Wilmington anticline fold axis.

The maximum relief along the strike of the Wilmington anticline is ~63 m on the Bent Spring formation. This was measured as the total structural relief on the Bent Spring formation and implies about 118 m of slip on the underlying Wilmington thrust. Based on the fault dip, this yields a slip rate of 0.23-0.59 mm/yr for the past ~200-500 ka. Our analysis does not require a component of strike slip on the Wilmington fault. However, oblique, right-lateral reverse motion has been proposed on the larger THUMS-Huntington Beach system, suggesting the possibility of a strike-slip component of motion on the Wilmington fault (Ishutov, 2013; Wright, 1991; Truex, 1974). If this is the case, the dip-slip rate calculated here should be considered a minimum estimate.

Earthquake Hazard
Our 3D fault model allows us to calculate the areas of the Wilmington fault and neighboring structures to estimate the maximum magnitudes of earthquakes they may generate. For this assessment, we use published empirical relations between rupture area and moment magnitude (Hanks and Bakun, 2008, 2002; Biasi and Weldon, 2006; Wells and Coppersmith, 1994). The 3D seismic survey constrains interpretation of the fault to depths of ~5-7 km based on truncations of stratigraphic horizons. Our mapping defined an envelope of permissible dip magnitudes to project the fault to greater depths and yielded a 3D representation of the fault from which to derive fault surface area. Our preferred fault dip (32°) yields a fault surface area of ~170 km^2, whereas the range of permissible fault dips (14-50°) yields possible fault surface areas of ~158-208 km^2. In all cases, the fault appears to intersect either the Newport-Inglewood strike-slip fault or Compton-Los Alamitos thrust ramp above the base of seismicity in the Community Fault Model (CFM) (Plesch et al., 2007). Although mechanical linkage of these faults is likely, suggesting the potential for large dynamic ruptures, these fault intersections were used to define the limits of the Wilmington fault area for hazard calculations.

On the basis of empirical relations between fault rupture area and magnitude and the range of fault area estimates (158-208 km^2), ruptures on the Wilmington blind-thrust could generate a M 6.2-6.3 earthquake (Table 1). Moreover, the Wilmington blind-thrust may also be linked to faults both along strike and down-dip, enabling larger, multi-segment earthquakes. For example, the Huntington Beach anticline and fault system extend south from the Wilmington structure forming part of the THUMS-Huntington Beach system (Ishutov, 2013; Legg et al., 2007; Wright, 1991, 1987; Henry, 1987; Truex, 1974). Our mapping suggests that these two structures represent part of an *en échelon*, oblique-slip thrust fault. Ishutov (2013) documented deformed Quaternary strata above the southern extent of the Huntington Beach segment, which indicates

that this fault segment is also tectonically active along with the Wilmington blind-thrust. Thus, the possibility exists for larger, multi-segment earthquakes on the Wilmington and Huntington Beach system, similar to the rupture pattern in the 2008 M 7.9 Wenchuan earthquake (Hubbard et al., 2014, 2010; Hartzell et al., 2013; Qi et al., 2011; Hubbard and Shaw, 2009; Liu-Zeng et al., 2009; Magistrale and Day, 1999). If the Wilmington and Huntington Beach segments ruptured simultaneously, they could generate a M 6.5 event.

The Torrance anticline lies along strike to the north of the Wilmington structure and thus may represent an *en échelon*, along-strike extension of the Wilmington blind-thrust. However, no studies have yet defined the level of activity on this fault system. Nevertheless, if the Torrance, Wilmington, and Huntington Beach segments all ruptured together, they could produce M 6.7-6.8 earthquakes.

Table 1. Possible single- and multi-segment rupture scenarios. Magnitude is calculated using empirical relations between rupture area and moment magnitude and average displacement is calculated using empirical relations between magnitude and average displacement (Hanks and Bakun, 2008, 2002; Biasi and Weldon, 2006; Wells and Coppersmith, 1994). The recurrence interval is calculated using slip rates of 0.23-0.59 mm/yr determined for the Wilmington blind-thrust preferred dip.

Fault Segments	Area (km^2)	Magnitude (M$_w$)	Avg. Displacement (m)	Recurrence Interval (yrs.)
Wilmington				
Preferred Dip (32°)	170.53	6.21	0.54	911-2336
Minimum Dip (14°)	158.28	6.18	0.52	885-2271
Maximum Dip (50°)	208.25	6.30	0.58	983-2521
Wilmington Preferred Dip +				
Torrance Segment	432.64	6.62	0.77	1298-3330
Huntington Beach (HB) Segment	355.18	6.53	0.71	1204-3089
Torrance and HB Segments	617.29	6.79	0.89	1513-3881
Wilmington Preferred Dip +				
(Torrance Segment and HB Segments) +				
Compton Thrust	971.76	7.05	1.12	1905-4888
Newport Inglewood Fault	1408.81	7.27	1.36	2301-6401
Compton Thrust and Newport Inglewood Fault	1736.28	7.40	1.52	2579-7064

All of the scenarios above are based solely on rupture of thrust ramps that lie above the Compton blind-thrust fault, which they at depths of 6-10 km. This raises the possibility that the Wilmington thrust and its along-strike extensions represent splay in the hanging wall of the Compton thrust, and that the two faults may rupture together in large (M > 7.1) earthquakes.

Several large thrust fault earthquakes, including the 1999 Chi-Chi, Taiwan (M 7.8) and 2016 Kaikoura, New Zealand (M 7.8) events have involved similar linked rupture of low-angle thrust systems and hanging wall fault splays (Wang et al., 2018; Cesca et al., 2017; Hollingsworth et al., 2017; Yue et al., 2005; Shin et al., 2000). Similarly, possible interactions between the Wilmington fault and the Newport-Inglewood trend present the possibility of combined thrust and strike-slip ruptures (M > 7.3), such as occurred in the 2002 Denali, Alaska (M 7.9) earthquake (Eberhart-Phillips et al., 2003).

Given the range of fault slip rates from 0.23.0.59 mm/year over the past ~200-500 ka, and assuming that this slip is released in M 6.2-6.3 earthquakes, the Wilmington blind-thrust could have an average recurrence interval time of ~885-2520 years (Table 1) (Hanks and Bakun, 2008, 2002; Biasi and Weldon, 2006; Wells and Coppersmith, 1994). Multi-segment ruptures, including simultaneous rupture of the Torrance and Huntington Beach segments (M 6.7-6.8), would occur less frequently, with a recurrence interval ranging from ~1513-3881 years. Similarly, ruptures of the Wilmington blind-thrust and the Compton (M 7.1) or Newport-Inglewood (M 7.3) faults would have an average recurrence interval time of ~1905-7065 years.

Given this potential, the Wilmington blind-thrust represents a significant, deterministic seismic hazard in southern California. Even moderate-magnitude earthquakes could cause considerable damage given their location directly beneath the densely populated Los Angeles metropolitan area (home to ~13 million people) and the Ports of Los Angeles and Long Beach (busiest port in the U.S. and the fifth-busiest port in the world). The Wilmington fault's potential linkage with other structures in the region, its reverse component of slip, its increasing slip rate, and its location within a deep sedimentary basin may compound the seismic hazard and pose the threat of local tsunamis (Bohannon and Gardner, 2004; Field, 2001, 2000). Additionally, it has been shown that reverse or oblique-reverse coseismic displacements may increase ground motions by 50% relative to rupture on a vertical strike-slip fault (Abrahamson and Somerville, 1996; Somerville et al., 1996). Recent ruptures on similar geologic structures in the region, including the 1971 San Fernando (M 6.6) and 1994 Northridge (M 6.7) earthquakes have caused significant casualties and billions in damages (Tsutsumi and Yeats, 1999; Hauksson et al., 1995). Thus, consideration of this fault in seismic hazard assessments is important for efforts to ensure the safety of the densely populated and economically important Los Angeles metropolitan and harbor regions.

Summary of Results
In summary, this effort has yielded new 3D fault models for the Wilmington blind-thrust, and the Huntington Beach and Torrance Anticline fault segments. New geologic horizon models of Late Miocene to Holocene sedimentary units have also been created to aid in understanding the basin architecture and deformational history of the active fault strands in the region.

Our analysis reveals that the Wilmington thrust is a blind fault that was reactivated at post 571 ka, and is capable of generating an M 6.2-6.3 earthquake with a recurrence interval of ~885-2520

years. The fault is likely linked to other active structures, both down-dip and along strike, which increases the hazard posed by a potential rupture.

This study will be used as a basis for defining the Late Quaternary activity, slip rate, and earthquake potential (Mmax) of the Wilmington blind-thrust providing a basis for its inclusion in earthquake source models and regional seismic hazard assessments. Moreover, this study refined our understanding of the interactions between the Wilmington blind-thrust and other earthquake sources in the Los Angeles basin (e.g., Compton, Newport Inglewood), thereby helping to improve the internal consistency and accuracy of regional seismic hazards assessment.

Our results will be disseminated through peer-reviewed publications, as well as by incorporation of new fault representations in the SCEC Community Fault Model (CFM) (Plesch et al., 2007). We are currently finalizing a manuscript for submission. Data and models will also be provided for inclusion in the California Reference Fault Parameter Database (e.g., Dawson, 2013), and the USGS Fault and Fold database. Providing new fault representations through these mechanisms will enable researchers studying dynamic rupture process, as well as those simulating earthquake wave propagation for strong ground motion prediction using finite source representations, to incorporate the Wilmington blind-thrust fault into their models.

References

Abrahamson, N.A., Somerville, P., 1996. Effects of the Hanging Wall and Footwall on Ground Motions Recorded during the Northridge Earthquake. Bull. Seismol. Soc. Am. 86.

Allmendinger, R.W., 1998. Inverse and forward numerical modeling of trishear fault-propagation folds. Tectonics 17, 640–656. https://doi.org/10.1029/98TC01907

Baher, S., Fuis, G., Sliter, R., Normark, W.R., 2005. Upper-Crustal Structure of the Inner Continental Borderland near Long Beach, California. Bull. Seismol. Soc. Am. 95, 1957–1969. https://doi.org/10.1785/0120040051

Biasi, G.P., Weldon, R.J., 2006. Estimating Surface Rupture Length and Magnitude of Paleoearthquakes from Point Measurements of Rupture Displacement. Bull. Seismol. Soc. Am. 96, 1612–1623. https://doi.org/10.1785/0120040172

Bohannon, R.G., Gardner, J.V., 2004. Submarine landslides of San Pedro Escarpment, southwest of Long Beach, California. Mar. Geol., Submarine-slump-generated Tsunamis 203, 261–268. https://doi.org/10.1016/S0025-3227(03)00309-8

Cesca, S., Zhang, Y., Mouslopoulou, V., Wang, R., Saul, J., Savage, M., Heimann, S., Kufner, S.-K., Oncken, O., Dahm, T., 2017. Complex rupture process of the Mw 7.8, 2016, Kaikoura earthquake, New Zealand, and its aftershock sequence. Earth Planet. Sci. Lett. 478, 110–120. https://doi.org/10.1016/j.epsl.2017.08.024

Davis, T.L., Namson, J.S., 1998. Southern and central coastal California cross section map.

Dolan, J.F., Christofferson, S.A., Shaw, J.H., 2003. Recognition of paleoearthquakes on the Puente Hills blind thrust fault, California. Science 300, 115–118. https://doi.org/10.1126/science.1080593

Eberhart-Phillips, D., Haeussler, P.J., Freymueller, J.T., Frankel, A.D., Rubin, C.M., Craw, P., Ratchkovski, N.A., Anderson, G., Carver, G.A., Crone, A.J., Dawson, T.E., Fletcher, H., Hansen, R., Harp, E.L., Harris, R.A., Hill, D.P., Hreinsdóttir, S., Jibson, R.W., Jones, L.M., Kayen, R., Keefer, D.K., Larsen, C.F., Moran, S.C., Personius, S.F., Plafker, G., Sherrod, B., Sieh, K., Sitar, N., Wallace, W.K., 2003. The 2002 Denali Fault Earthquake, Alaska: A Large Magnitude, Slip-Partitioned Event. Science 300, 1113–1118. https://doi.org/10.1126/science.1082703

Ehman, E.D., Edwards, B.D., 2017. Defining Aquifer Architecture Using Seismic and Sequence Stratigraphy in the Los Angeles Basin, California: a Foundation for Future Assessment and Management of Groundwater Resources. Am. Assoc. Pet. Geol.

Erslev, E.A., 1991. Trishear fault-propagation folding. Geology 19, 617–620. https://doi.org/10.1130/0091-7613(1991)019<0617:TFPF>2.3.CO;2

Field, E.H., 2001. Earthquake ground-motion amplification in Southern California (USGS Numbered Series No. 2001–164), Open-File Report. USGS.

Field, E.H., 2000. Accounting for Site Effects in Probabilistic Seismic Hazard Analyses of Southern California: Overview of the SCEC Phase III Report. Bull. Seismol. Soc. Am. 90, S1–S31. https://doi.org/10.1785/0120000512

Field, E.H., Biasi, G.P., Bird, P., Dawson, T.E., Felzer, K.R., Jackson, D.D., Johnson, K.M., Jordan, T.H., Madden, C., Michael, A.J., Milner, K.R., Page, M.T., Parsons, T., Powers, P.M., Shaw, B.E., Thatcher, W.R., Weldon, R.J., Zeng, Y., 2013. Uniform California earthquake rupture forecast, version 3 (UCERF3)—The time-independent model. US Geol. Surv. Open-File Rep. 2013–1165 Calif. Geol. Surv. Spec. Rep. 228 South. Calif. Earthq. Cent. Publ. 1792 Special Report 228, 97.

Fisher, M.A., Normark, W.R., Langenheim, V.E., Calvert, A.J., Sliter, R., 2004. The offshore Palos Verdes fault zone near San Pedro, Southern California. Bull. Seismol. Soc. Am. 94, 25.

Francis, R., Legg, M., 2007. Late Quaternary uplift of the Palos Verdes tectonic block; evidence from high resolution seismic imaging of the Palos Verdes Fault on the San Pedro Shelf, in: Geologic Guide Book, Geology and Paleontology of Palos Verdes Hills, California; a 60th Anniversary Revisit to Commemorate the 1946 Publication of U. S. Geological Survey Professional Paper 207. pp. 189–222.

Hanks, T.C., Bakun, W.H., 2008. M-logA Observations for Recent Large Earthquakes. Bull. Seismol. Soc. Am. 98, 490–494. https://doi.org/10.1785/0120070174

Hanks, T.C., Bakun, W.H., 2002. A bilinear source-scaling model for M − log A observations of continental earthquakes. Bull. Seismol. Soc. Am. 92, 1841–1846.

Hartzell, S., Mendoza, C., Ramirez-Guzman, L., Zeng, Y., Mooney, W., 2013. Rupture History of the 2008 Mw 7.9 Wenchuan, China, Earthquake: Evaluation of Separate and Joint Inversions of Geodetic, Teleseismic, and Strong-Motion Data. Bull. Seismol. Soc. Am. 103, 353–370. https://doi.org/10.1785/0120120108

Hauksson, E., Jones, L.M., Hutton, K., 1995. The 1994 Northridge earthquake sequence in California: Seismological and tectonic aspects. J. Geophys. Res. Solid Earth 100, 12335–12355. https://doi.org/10.1029/95JB00865

Henry, M.J., 1987. Los Angeles Basin – An Overview, in: Oil Producing Areas in Long Beach. Pacific Section of American Association of Petroleum Geologists, pp. 1–29.

Hollingsworth, J., Ye, L., Avouac, J.-P., 2017. Dynamically triggered slip on a splay fault in the Mw 7.8, 2016 Kaikoura (New Zealand) earthquake. Geophys. Res. Lett. 44, 2016GL072228. https://doi.org/10.1002/2016GL072228

Hubbard, J., Shaw, J.H., 2009. Uplift of the Longmen Shan and Tibetan plateau, and the 2008 Wenchuan (M= 7.9) earthquake. Nature 458, 194–7. https://doi.org/10.1038/nature07837

Hubbard, J., Shaw, J.H., Dolan, J.F., Pratt, T.L., McAuliffe, L.J., Rockwell, T.K., 2014. Structure and seismic hazard of the Ventura Avenue anticline and Ventura fault, California:

Prospect for large, multisegment ruptures in the Western Transverse Ranges. Bull. Seismol. Soc. Am. 104, 10701087. https://doi.org/10.1785/0120130125

Hubbard, J., Shaw, J.H., Klinger, Y., 2010. Structural Setting of the 2008 M-w 7.9 Wenchuan, China, Earthquake. Bull. Seismol. Soc. Am. 100, 2713–2735.

Hughes, A., Shaw, J.H., 2014. Fault displacement-distance relationships as indicators of contractional fault-related folding style. AAPG Bull. 98, 227–251. https://doi.org/10.1306/05311312006

Ishutov, S., 2013. Tectonic characterization of the THUMS-Huntington Beach fault, offshore southern California (Master's Thesis). California State University, Long Beach.

Legg, M., Prior, S., 2007. Wilmington Structure, Long Beach, California: a Strike-Slip Restraining Bend Popup? AAPG Search Discov. Artic. AAPG Annual Convention & Exhibition.

Legg, M.R., Goldfinger, C., Kamerling, M.J., Chaytor, J.D., Einstein, D.E., 2007. Morphology, structure and evolution of California Continental Borderland restraining bends. Geol. Soc. Lond. Spec. Publ. 290, 143–168. https://doi.org/10.1144/SP290.3

Liu-Zeng, J., Zhang, Z., Sun, J., Wen, L., Tapponnier, P., Xing, X., Xu, Q., Hu, G., Zeng, L., Ding, L., Ji, C., Hudnut, K., 2009. Co-seismic ruptures of the 12 May, 2008, Mw 8.0 Wenchuan earthquake, Sichuan: EW crustal shortening on oblique, parallel thrusts along the eastern edge of Tibet. Earth Planet. Sci. Lett. 286, 335–370.

Magistrale, H., Day, S., 1999. 3D simulations of multi-segment thrust fault rupture. Geophys. Res. Lett. 26, 2093–2096. https://doi.org/10.1029/1999GL900401

Mallet, J.-L., 1992. Discrete smooth interpolation in geometric modelling. Comput.-Aided Des. 24, 178–191. https://doi.org/10.1016/0010-4485(92)90054-E

McDougall, K., Hillhouse, J., Powell, C., II, Mahan, S., Wan, E., and Sarna-Wojcicki, A.M., 2012, Paleontology and geochronology of the Long Beach core sites and monitoring wells, Long Beach, California: U.S. Geological Survey Open-File Report 2011–1274, 235 p., 18 plates. https://pubs.usgs.gov/of/2011/1274/

Plesch, A., Shaw, J.H., Benson, C., Bryant, W.A., Carena, S., Cooke, M., Dolan, J., Fuis, G., Gath, E., Grant, L., Hauksson, E., Jordan, T., Kamerling, M., Legg, M., Lindvall, S., Magistrale, H., Nicholson, C., Niemi, N., Oskin, M., Perry, S., Planansky, G., Rockwell, T., Shearer, P., Sorlien, C., Suss, M.P., Suppe, J., Treiman, J., Yeats, R., 2007. Community Fault Model (CFM) for Southern California. Bull. Seismol. Soc. Am. 97, 1793–1802. https://doi.org/10.1785/0120050211

Ponti, D.J., Ehman, E.D., Edwards, B.D., Tinsley, J.C., Hildenbrand, T., Hillhouse, J.W., Hanson, R.T., McDougall, K., Powell, C.L., Wan, E., Land, M., Mahan, S., Sarna-Wojcicki, A.M., 2007. A 3-dimensional Model of Water-bearing Sequences in the Dominguez Gap Region, Long Beach, California. U.S. Geological Survey Open-File Report 2007-1017.

Pratt, T.L., Shaw, J.H., Dolan, J.F., Christofferson, S.A., Williams, R.A., Odum, J.K., Plesch, A., 2002. Shallow seismic imaging of folds above the Puente Hills blind-thrust fault, Los Angeles, California. Geophys. Res. Lett. 29, 18–1. https://doi.org/10.1029/2001GL014313

Qi, W., Xuejun, Q., Qigui, L., Freymueller, J., Shaomin, Y., Caijun, X., Yonglin, Y., Xinzhao, Y., Kai, T., Gang, C., 2011. Rupture of deep faults in the 2008 Wenchuan earthquake and uplift of the Longmen Shan. Nat. Geosci. 4, 634. https://doi.org/10.1038/ngeo1210

Shaw, J.H., Plesch, A., Dolan, J.F., Pratt, T.L., Fiore, P., 2002. Puente Hills blind-thrust system, Los Angeles, California. Bull. Seismol. Soc. Am. 92, 15.

Shaw, J.H., Suppe, J., 1996. Earthquake hazards of active blind-thrust faults under the central Los Angeles basin, California. J. Geophys. Res. 101, 8623–8642.

Shaw, J.H., Suppe, J., 1994. Active faulting and growth folding in the eastern Santa Barbara Channel, California. Geol. Soc. Am. Bull. 106, 607. https://doi.org/10.1130/0016-7606(1994)106<0607:AFAGFI>2.3.CO;2

Shin, T.C., Kuo, K.W., Lee, W.H.K., Teng, T.L., Tsai, Y.B., 2000. A Preliminary Report on the 1999 Chi-Chi (Taiwan) Earthquake. Seismol. Res. Lett. 71, 24–30. https://doi.org/10.1785/gssrl.71.1.24

Somerville, P., Saikia, C., Wald, D., Graves, R., 1996. Implications of the Northridge earthquake for strong ground motions from thrust faults. Bull. Seismol. Soc. Am. 86.

Stein, R.S., Ekström, G., 1992. Seismicity and geometry of a 110-km-long blind thrust fault 2. Synthesis of the 1982–1985 California Earthquake Sequence. J. Geophys. Res. 97, 4865–4883. https://doi.org/10.1029/91JB02847

Stein, R.S., King, G.C., 1984. Seismic potential revealed by surface folding: 1983 Coalinga, California, earthquake. Science 224, 869–872. https://doi.org/10.1126/science.224.4651.869

Suppe, J., Medwedeff, D., 1990. Geometry and kinematics of fault-propagation folding. Eclogae Geol. Helvetiae 83, 409–454.

Truex, J.N., 1974. Structural Evolution of Wilmington, California, Anticline. AAPG Bull. 58, 2398–2410.

Tsutsumi, H., Yeats, R.S., 1999. Tectonic setting of the 1971 Sylmar and 1994 Northridge earthquakes in the San Fernando Valley, California. Bull. Seismol. Soc. Am. 89, 1232–1249.

Wang, T., Wei, S., Shi, X., Qiu, Q., Li, L., Peng, D., Weldon, R.J., Barbot, S., 2018. The 2016 Kaikōura earthquake: Simultaneous rupture of the subduction interface and overlying faults. Earth Planet. Sci. Lett. 482, 44–51. https://doi.org/10.1016/j.epsl.2017.10.056

Wells, D., Coppersmith, K., 1994. New Empirical Relationships among Magnitude, Rupture Length, Rupture Width, Rupture Area, and Surface Displacement. Bull. Seismol. Soc. Am. 84, 974–1002.

Wright, T.L., 1991. Structural Geology and Tectonic Evolution of the Los Angeles Basin, California, Memoir 52. ed. American Association of Petroleum Geologists, Tulsa, Oklahoma.

Wright, T.L., 1987. Structural geology and tectonic evolution of the Los Angeles Basin, California, in: AAPG Bulletin. https://doi.org/10.1306/9488784D-1704-11D7-8645000102C1865D

Yue, L.-F., Suppe, J., Hung, J.-H., 2005. Structural geology of a classic thrust belt earthquake: the 1999 Chi-Chi earthquake Taiwan (Mw=7.6). J. Struct. Geol. 27, 2058–2083. https://doi.org/10.1016/j.jsg.2005.05.020